A Study of the Crystal Dynamics of Zinc

G. BORGONOVI, G. CAGLIOTI, AND J. J. ANTAL*
Comitato Nazionale per l'Energia Nucleare, C.C.R. Euratom, Ispra, Varese, Italy
(Received 14 June 1963)

A number of the normal modes of vibration of the anisotropic hexagonal metallic system of zinc have been studied through a determination of the dispersion relations by neutron inelastic scattering. Measurements carrying relatively small experimental errors have been made for directions in a single crystal which produce information about the motions of atoms within the basal planes, the motion of the basal planes acting as single units, and the motions of atoms perpendicular to the basal planes which tend to warp these planes. Attempts are made to fit the experimental data to formulations of Born-von Kármán dynamical theory involving generalized forces between pairs of atoms. Consideration of forces extending to fourth nearest neighbors is necessary to obtain agreement with our dispersion relations. The experimental data generally supply details of the anisotropic mechanisms operating in zinc and indicate that anomalies might exist in the dispersion relations describing atomic motions perpendicular to the basal planes.

INTRODUCTION

A PROGRAM of research involving a study of the dispersion relations of the anisotropic system of zinc is reported here. Extensive measurements with relatively high resolution of the normal modes of vibration of zinc have been made on a triple axis neutron spectrometer using the method employing a constant scattering vector $\mathbf{Q}$. Zinc is a good choice inasmuch as it is strongly anisotropic for a metal; the c/a ratio of this hexagonal crystal is 1.85, it cleaves easily along the basal plane, and it has an anisotropic electrical conductivity and thermal expansion. The thermal neutron scattering cross section of zinc is almost totally coherent and its capture cross section is small. Also, large single crystals of zinc are commercially available.

With two atoms per unit cell, and a symmetry lower than cubic, zinc will give rise to optical as well as acoustical branches in the relations between frequency ν and wave vector $\mathbf{q}$ describing the phonons in the crystal. The range of values of ν and $\mathbf{q}$ for zinc lies well within the working region of the triple-axis spectrometer.

It will be shown that attempts to fit the experimental data to expressions developed from Born-von Kármán theory may be considered to be successful. In this respect the present work seems to overcome difficulties experienced by other authors in fitting more or less elaborate models, within the Born-von Kármán theory, to hexagonal metals such as zinc,[1] magnesium,[2,3] and beryllium[4]; since our experimental errors are generally small, it seemed to us reasonable, after the failure of the simplest models, to use a more elaborate calculation, though involving a higher number of parameters.

THEORETICAL BACKGROUND

The method of neutron inelastic scattering as applied to the study of lattice dynamics is well established.[5–7] The starting point is always the necessity of satisfying the momentum and energy conservation laws in the interaction between a neutron of initial energy E_0, and a phonon of energy $h\nu$ and wave vector $\mathbf{q}$. Accordingly, we have the expressions

$$\begin{aligned}\mathbf{Q}\equiv\mathbf{k}_0-\mathbf{k}'&=2\pi\boldsymbol{\tau}-\mathbf{q}\,,\\ E_0-E'&=\pm h\nu\,.\end{aligned}\tag{1}$$

The incoming and outgoing neutron wave vectors are $\mathbf{k}_0$ and $\mathbf{k}'$, respectively, and the outgoing neutron energy is E'. The reciprocal lattice vector $\boldsymbol{\tau}$ locates the region of study in reciprocal space. The intensity of the neutron scattering process is governed by[8–12]

$$\frac{k'}{k_0}\begin{Bmatrix}N+1\\ N\end{Bmatrix}e^{-2W}g_j^2(\mathbf{q},\boldsymbol{\tau})\,,\tag{2}$$

where $N=[\exp(h\nu/K_BT)-1]^{-1}$ is the Boltzmann population factor for the process (K_B and T are the Boltzmann constant and absolute temperature) where the neutron gains energy from the lattice [$-h\nu$ in Eq. (1)], and $N+1$ is the corresponding factor for an energy loss process [$+h\nu$ in Eq. (1)]. e^{-2W} is the usual Debye-Waller factor and $g_j^2(\mathbf{q},\boldsymbol{\tau})$ is a sort of structure factor

* Visiting scientist from U. S. Army Materials Research Agency, Watertown, Massachusetts, under a Secretary of the Army's Research and Study Fellowship.

[1] E. Maliszewski, Phys. Letters. **1**, 338 (1962).

[2] P. K. Iyengar, G. Venkataraman, K. R. Rao, P. R. Vijayaraghavan, and A. P. Roy, in *Proceedings of the Chalk River Symposium on Inelastic Scattering of Neutrons in Solids and Liquids* (International Atomic-Energy Agency, Vienna, 1963), Vol. II, p. 99.

[3] M. F. Collins, Proc. Phys. Soc. (London) **80**, 362 (1962).

[4] R. E. Schmunk, R. M. Brugger, P. D. Randolph, and K. A. Strong, Phys. Rev. **128**, 562 (1962).

[5] B. N. Brockhouse, in *Proceedings of the Symposium on the Inelastic Scattering of Neutrons in Solids and Liquids* (International Atomic-Energy Agency, Vienna, 1960), p. 113.

[6] B. N. Brockhouse, T. Arase, G. Caglioti, K. R. Rao, and A. D. B. Woods, Phys. Rev. **128**, 1099 (1962).

[7] K. E. Larsson, U. Dahlborg, and S. Holmryd, Arkiv Fysik **17**, 369 (1960).

[8] R. Weinstock, Phys. Rev. **65**, 1 (1944).

[9] B. N. Brockhouse and P. K. Iyengar, Phys. Rev. **111**, 347 (1958).

[10] I. Waller and P. O. Froman, Arkiv Fysik **4**, 183 (1952).

[11] P. O. Froman, Arkiv Fysik **4**, 191 (1952).

[12] B. N. Brockhouse, L. N. Becka, K. R. Rao, and A. D. B. Woods, in *Proceedings of the Chalk River Symposium on Inelastic Scattering of Neutrons in Solids and Liquids* (International Atomic-Energy Agency, Vienna, 1963), Vol. II, p. 23.

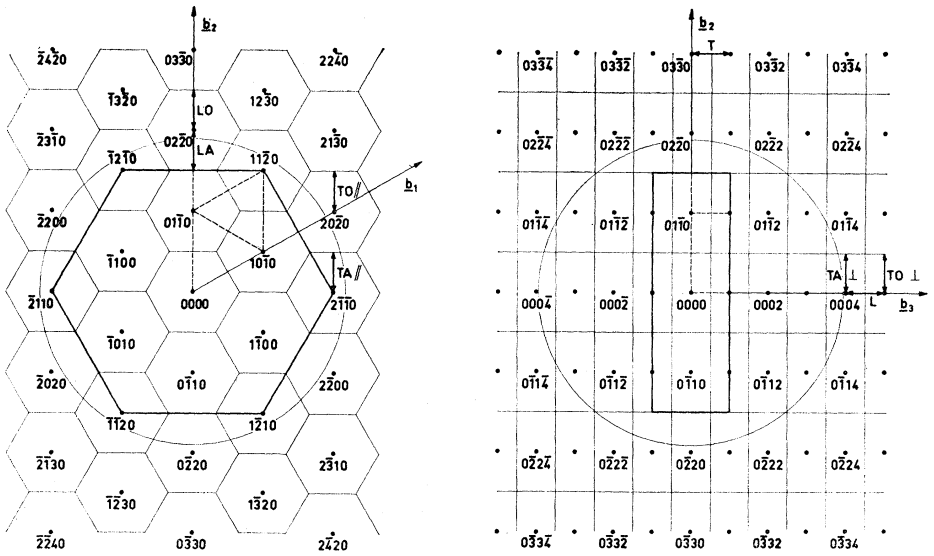

FIG. 1. The $(\mathbf{b}_1,\mathbf{b}_2)$ and $(\mathbf{b}_2,\mathbf{b}_3)$ reciprocal lattice planes. The bold lines enclose the area in which the structure factor repeats. Within this area dashed lines, as far as the structure factor is concerned, are equivalent to the lines covered by the measurements, the latter being indicated by arrows. The elastic circle of radius k_0 is also indicated.

given by the expression

$$g_j^2(\mathbf{q},\tau)=|\sum_p b_p[\mathbf{Q}\cdot\mathbf{C}_j(\mathbf{q},p)] \times[\nu_j(\mathbf{q})]^{1/2}\exp(i\mathbf{Q}\cdot\mathbf{R}_p)|^2. \quad (3)$$

In this equation $p=1,2$ specifies the atom in the unit cell, $\mathbf{R}_p$ is its position vector, b_p is its scattering amplitude, and $\mathbf{C}_j(\mathbf{q},p)$ is the polarization vector for the branch j which can be obtained once the frequency versus wave-vector dispersion relation $\nu_j(\mathbf{q})$ is determined.

Within Born-von Kármán theory, the $\nu_j(\mathbf{q})$ are given by the solutions of the secular equation

$$|D_{\alpha\beta}(\mathbf{q}|p,p')-4\pi^2\nu^2\delta_{\alpha\beta}\delta_{pp'}|=0, \quad (\alpha,\beta=1,2,3;\ p,p'=1,2),$$

where $D_{\alpha\beta}(\mathbf{q}|p,p')$ is the element of the dynamical matrix, relative to atoms of indices p and p', and Cartesian components α and β.

Zince has a hexagonal close-packed structure characterized by the parameters[13] $a=2.6648$ Å and $c=4.9467$ Å. We shall speak of the *basic vector* $\mathbf{R}_2$ as that which connects the two atoms in the unit cell proceeding from the point (0,0,0) to the point $(\frac{1}{3},\frac{2}{3},\frac{1}{2})$, referred to the hexagonal axes. Two reciprocal lattice planes can be drawn, normal to the $\mathbf{c}$ and $\mathbf{a}_1$ axes of the direct lattice (see Fig. 1). Waves travelling in the $[01\bar{1}0]$ and $[0001]$ directions, both longitudinal and transverse, of polarizations both perpendicular ($\perp$) and parallel ($/\!/$) to the basal planes, can then be studied.

We found it convenient to limit this study to wave vectors propagating along the $[01\bar{1}0]$ and the $[0001]$ symmetry directions. In these directions the secular determinant of Eq. (4) factors into three 2×2 determinants associated with pure longitudinal and transverse components.

Consideration of the geometry of the spectrometer and the incident neutron wavelength defines the general regions in the reciprocal planes where the experimental data is to be taken. The specific working points in the reciprocal lattice planes must be determined by an examination of the structure factor given in Eq. (3).

The general behavior of the structure factor seems to be relatively insensitive to the model one selects to describe the dynamical properties of the crystal, so that at first, use was made of the computations made by Iyengar *et al.*[2] for magnesium. Afterwards, using the simple model proposed by Begbie,[14,15] we obtained the curves given in Fig. 2 with force constants evaluated for zinc *a posteriori* from our neutron results. In Fig. 2, $g_j^2(\mathbf{q},\tau)$ is plotted in units of $bp^2|\mathbf{Q}\cdot\mathbf{C}_j(\mathbf{q},p)|^2/\nu_j(\mathbf{q})$ for the symmetry directions along which phonons were measured.

The structure factor is periodic in reciprocal space within the areas enclosed by bold lines in Fig. 1. The curves of Fig. 2 are equivalent to the lines in the reciprocal planes where the measurements were actually taken, indicated by labeled bold lines in Fig. 1.

THE EXPERIMENT

The measurements were performed at room temperature with the triple axis spectrometer previously described[16,17] installed at the 5-MW Ispra-1 reactor.

[13] R. W. G. Wyckoff, *Crystal Structures* (Interscience Publishers, Inc., New York, 1960).

[14] G. H. Begbie and N. Born, Proc. Roy. Soc. (London) **A188**, 179 (1946).

[15] G. H. Begbie, Proc. Roy. Soc. (London) **A188**, 189 (1946).

[16] G. Caglioti, E. De Agostino, F. Marsili, A. Paoletti, U. Pellegrini, and F. P. Ricci, Suppl. Nuovo Cimento, **23**, 17 (1962).

[17] G. Caglioti and P. Ascarelli, in *Proceedings of the Chalk River Symposium on Inelastic Scattering of Neutrons in Solids and Liquids* (International Atomic-Energy Agency, Vienna, 1963), Vol. I, p. 259.

Throughout the measurements the **Q=constant** method[5] was utilized with a constant-impinging wave vector $\mathbf{k}_0$ associated with a wavelength $\lambda=1.24_8$ Å. The monochromating and analyzing crystals, mounted in reflection, were cut from the same aluminum ingot, and the reflection used for both was the (111). Their mosaic spread was about 8′ (full width at half-maximum).

The Soller-type collimators had the following horizontal angular divergences: 20′, 25′, 70′, and 35′ for the in-pile, monochromator-sample, sample-analyzer, analyzer-BF_3 counter collimators, respectively.

Because of its immediate availability the 70′ collimator was employed in place of one with a lesser, more compatible divergence in this series experiments.[18] No serious difficulties were encountered with this arrangement, particularly when high-energy phonons were measured.

Any single measurement of a point on a dispersion curve was realized by counting the intensity at 34 positions of the scattering angle ϕ, the sample orientation ψ, and the analyzing angle $2\vartheta_A$, as computed with the IBM 7090 at this Center. The increments in ϕ were fixed during any single run at 3′, 6′, or 15′, while the smallest step for both ψ and $2\vartheta_A$ obtainable automatically was 5′.[19]

The zinc sample, a 2-in.-diam sphere,[20] had a mosaic spread of about 6′; it was heavily etched before starting the measurements.

The counting period was controlled by a low-efficiency monitor set in the monochromatic beam at the exit of the main shielding.[16] As a rule it was set so as to obtain about 300 counts above the background level at the maximum of the phonon peak. Typical phonons are shown in Fig. 3.

TABLE I. Experimental values of the frequencies with their experimental errors. Frequencies ν (in units 10^{12} sec^{-1}).

q/q_{max}	[0001] T Acoustical	[0001] T Optical	[01$\bar{1}$0] T// Acoustical	[01$\bar{1}$0] T// Optical	[01$\bar{1}$0] L Optical
0.00		2.26±0.08		2.19±0.06	2.20±0.06
0.10				2.19±0.08	2.41±0.06
0.20		2.21±0.07		2.36±0.12	2.66±0.05
0.30			1.59±0.08	2.46±0.06	3.19±0.05
0.40	1.00±0.07	2.13±0.06	2.10±0.08	2.67±0.05	3.88±0.06
0.50			2.50±0.08	2.92±0.05	4.50±0.08
0.60	1.35±0.07	2.12±0.06	2.85±0.08	3.17±0.08	5.14±0.10
0.70			3.07±0.08	3.40±0.08	5.70±0.05
0.80	1.63±0.07	2.02±0.06	3.35±0.07	3.63±0.10	6.09±0.05
0.90			3.46±0.07	3.63±0.08	6.20±0.08
1.00	1.83±0.06		3.47±0.08	3.68±0.05	6.25±0.06

q/q_{max}	[0001] L Acoustical	[0001] L Optical	[01$\bar{1}$0] T⊥ Acoustical	[01$\bar{1}$0] T⊥ Optical	[01$\bar{1}$0] L Acoustical
0.00		4.64±0.07		4.64±0.07	
0.10				4.67±0.08	
0.20	0.67±0.11	4.50±0.05	0.95±0.12	4.57±0.06	1.74±0.10
0.30			1.09±0.11	4.28±0.09	2.85±0.05
0.40	1.15±0.10	4.22±0.05	1.32±0.11	4.00±0.07	3.61±0.07
0.50			1.47±0.09	3.65±0.06	4.33±0.07
0.60	1.68±0.08	3.91±0.06	1.51±0.08	3.30±0.05	4.84±0.07
0.70	1.81±0.09		1.70±0.10	3.10±0.07	5.32±0.09
0.80	2.22±0.09	3.42±0.06	1.84±0.09	2.91±0.07	5.65±0.10
0.90	2.52±0.10		2.03±0.09	2.69±0.06	5.86±0.10
1.00	2.90±0.10		2.04±0.07	2.46±0.05	6.05±0.08

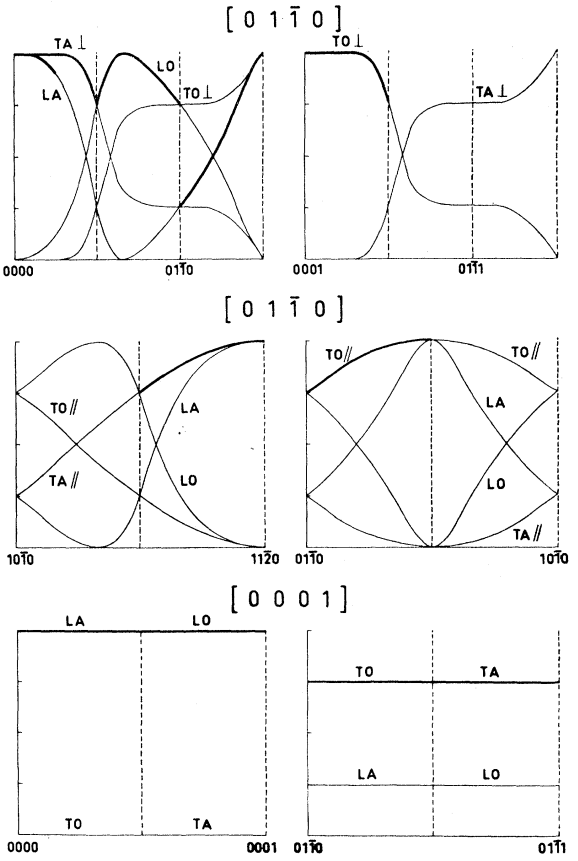

FIG. 2. The structure factor $g_j^2(\mathbf{q},\tau)$ calculated using the Begbie and Born model, along the dashed lines of Fig. 1. The bold lines are associated with the lines along which measurements were taken (see Fig. 1). For the [01$\bar{1}$0]L and [01$\bar{1}$0]T// branches, the structure factor depends on the force constants λ and μ of Begbie, assumed to be $\lambda=1.3\times10^3$ dyn/cm and $\mu=-0.75\times10^3$ dyn/cm as deduced from a preliminary best fit (see text).

THE RESULTS

In Table I we give the $\nu_j(\mathbf{q})$ values experimentally determined for longitudinal and transverse branches in the [01$\bar{1}$0] and [0001] symmetry directions. These values are plotted in Fig. 4.

Although the Born–von Kármán approach to a solution of the problem of lattice dynamics in crystals was found to be inadequate in the majority of problems investigated to date, its simplicity recommends it as a starting point in an analysis of the present data. We have attempted to fit our experimental data with two different extensions of the Born–von Kármán theory; namely those of Begbie and Born,[14,15] and Collins.[3] Both solutions have been applied to the hexagonal system.

[18] As a general rule, it would appear that the sample-analyzer collimator should have a divergence that is not less than the monochromator-sample collimator if the instrument is to cover, in a realistic way [note the statistical factors in Eq. (2)], the range of energy changes usually encountered.

[19] The maximum value for ϕ utilized during this experiment was 120 deg, while $2\vartheta_A$ (which in our instrument can reach a value of 90 deg) was usually kept in the range 25 deg $\lesssim 2\vartheta_A \lesssim$ 45 deg.

[20] Supplied by Metals Research Ltd., Cambridge, England.

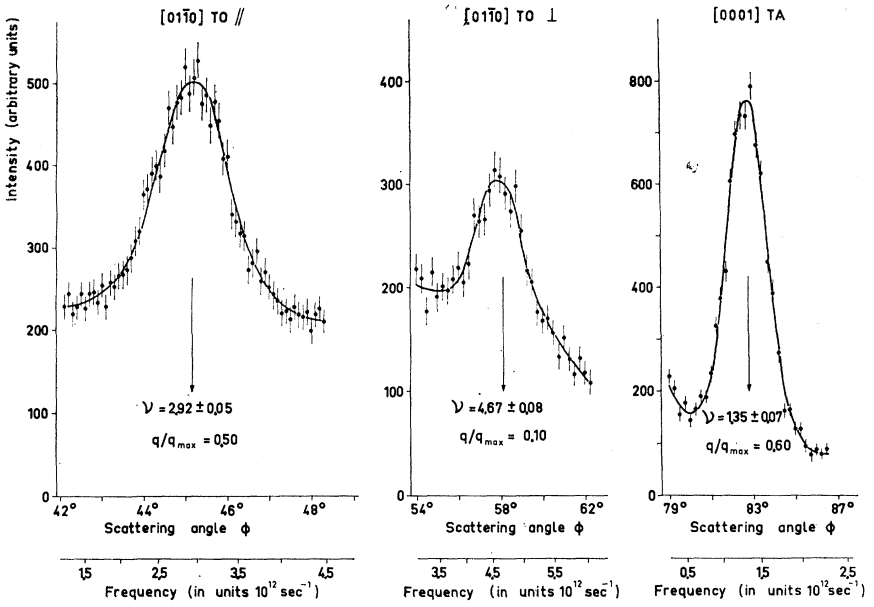

FIG. 3. Typical phonon patterns. Statistical experimental errors are indicated, together with the assumed error in the frequency. This error is reported in Table I and appears in Fig. 4.

The calculation of Begbie and Born is based upon generalized forces among first and second nearest neighbors. Seven independent interatomic force constants result which are related to the elastic constants through a system of five equations. In principle, the data presented here should allow the determination of six of the seven interatomic force constants as indicated in Table II.

The calculation by Collins is based upon generalized forces extended to include third and fourth nearest neighbors. Thirteen independent interatomic force constants result which are related to the elastic constants through a similar system of five equation. In principle, the data presented here should allow the determination of eleven of the thirteen interatomic force constants, also listed in Table II. Least-squares fits to the experimental data were attempted for both calculations using the IBM-7090 computer. The experimentally determined elastic constants were not introduced in the fit, so that the fitted curves are based solely upon data determined by neutron scattering. The slopes of the dispersion relations for small values of $\mathbf{q}$ as given by the elastic constants have been inserted in Fig. 4 to allow visual comparison with the neutron data.

TABLE II. Force constants involved in theoretical description of the dispersion relations studied.

Branch	Second nearest-neighbor theory[a]	Fourth nearest-neighbor theory[b]
[01$\bar{1}$0] L [01$\bar{1}$0] T//	$\alpha, \beta, \lambda, \mu$	$B_1, B_2, G_1, G_2, \alpha, A_1$
[0001] T	λ	B_1, B_2, G_1, G_2, D_1
[01$\bar{1}$0] T⊥	ν, γ	B_3, G_3, A_2
[0001] L	ν	B_3, G_3, δ

[a] G. H. Begbie, see Ref. 15.
[b] M. F. Collins, see Ref. 3.

An attempt was made to fit the Begbie and Born solution with the experimental data obtained with the crystal oriented with its c axis perpendicular to the plane of scattering. These data include the acoustical and optical branches designated [01$\bar{1}$0] L and [01$\bar{1}$0] T// which involve vibrations in the basal plane only. It was not possible to fit the experimental data with a unique set of the force constants α, β, λ, and μ within the experimental errors. It was possible, however, to fit both the longitudinal dispersion curves with one set of constants and the two transverse dispersion curves with another set of force constants. Apparently, this is the limit of applicability of the Begbie and Born formulation to this hexagonal system. Accordingly, it was not possible to find unique values for ν, γ, and λ which would allow a fit with the experimental data for the [01$\bar{1}$0] T⊥, [0001] L, and [0001] T modes of vibration within the experimental error. The disagreement in these cases is even more acute.

A least-squares fit of the data to the formulation of Collins (generalized forces to fourth nearest neighbors) was more successful. It was possible to obtain a good fit to the experimental data for all six dispersion relations designated in Table II as [01$\bar{1}$0] L, [01$\bar{1}$0] T//, and [0001] T with a unique set of the seven force constants B_1, B_2, G_1, G_2, α, A_1, and D_1. This is three more constants over the Begbie and Born formulation. The constants are listed in Table III.

TABLE III. Interatomic force constants determined from consideration of forces to fourth nearest neighbors (in units of 10^9 dyn/cm).[a]

B_1	B_2	G_1	G_2	α	D_1	A_1	B_3	G_3	A_2	δ
0.75	2.25	−0.46	−1.2	25.4	−1.4	0.92	−5.0	−2.7	2.94	−2.9

[a] The order of magnitude of the errors corresponds to several units in the last significant figure of each constant.

The four force constants B_3, G_3, A_2, and δ, also listed in Table III, were obtained from a least-squares fit to the experimental data for the four $[01\bar{1}0]$ T$\perp$ and $[0001]$ L branches; the quality of this fit to the $[01\bar{1}0]$ TA$\perp$ phonons of small wave vector was poorer than anywhere else. In view of this fact, errors resulting from the geometry of the triple-axis experiment and from the determination of the central position of the phonon peaks were examined thoroughly for the $[01\bar{1}0]$ TA$\perp$ branch. The error bars assigned in Table I and Fig. 4, consequently, are thought to be proper and the more prominent deviations from monotonic curvature are believed to be real.

DISCUSSION AND CONCLUSIONS

Three other experimental determinations of the dispersion relations for zinc are the x-ray scattering data of Joynson[21] and some preliminary neutron scattering data of Maliszewski[1] and Maliszewski *et al.*[22] Our data are in agreement with that of Maliszewski for the $[0001]$ L branch, but lie between those of the above quoted authors for the $[01\bar{1}0]$ TA$\perp$ branch. The present data are in excellent agreement with the $[0001]$ T branch as determined by Joynson but are in general disagreement elsewhere.

Attempts to fit experimental data for hexagonal metals to the formulation of Begbie and Born have not been wholly successful. Collins, in a study of magnesium,[3] considered it necessary to include generalized forces to third and possibly fourth nearest neighbors. Schmunk, Brugger, Randolph, and Strong[4] felt that a combination of a central-force model for distant neighbors and generalized-force model for nearest neighbors would give an adequate description of their neutron data on beryllium.

As indicated in the previous section, the Begbie and Born formulation is not adequate in the case of the present data. It was necessary to seek a more elaborate model which included interactions amongst more distant neighbors. The extension by Collins of the generalized-force model to include third and fourth neighbors was explored. The following discussion will be based on the ability of this formulation to fit the present experimental data.

It is perhaps best to take advantage of the anisotropy peculiar to zinc to formulate a discussion in three parts: motions within the basal planes, motions of the basal planes as a whole, and motions tending to warp the basal planes.

Motions within the basal planes are represented by the branches $[01\bar{1}0]$ L and $[01\bar{1}0]$ T$/\!/$. A striking feature of these branches is the relatively high values

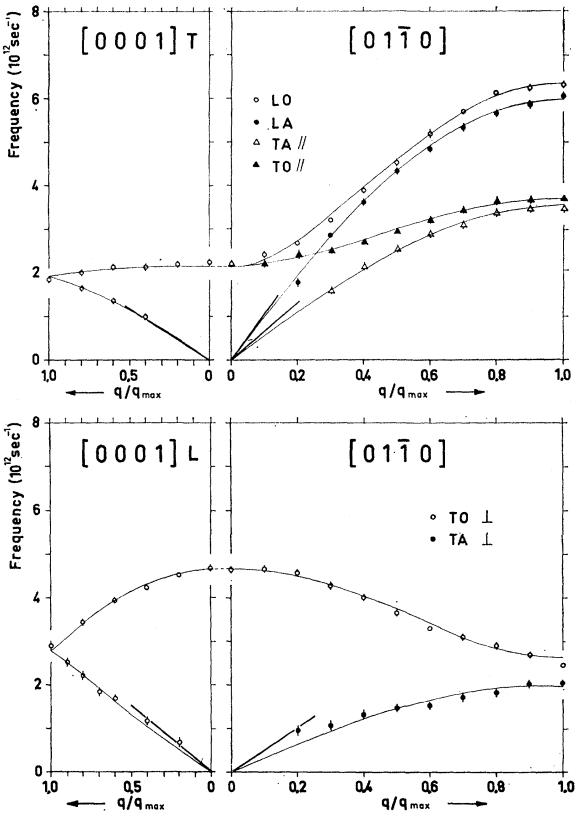

FIG. 4. Experimental dispersion curves for the $[01\bar{1}0]$ and $[0001]$ directions. The straight lines passing through zero were calculated from the elastic data of Alers and Neighbours (see Ref. 23). Full lines are the result of a least-square fit using the Born–von Kármán formulation of Collins (see Ref. 3).

of frequency reached at the zone boundary. In particular, for the $[01\bar{1}0]$ LO at $q/q_{\max}=1$, the frequency reaches a value of 6.25×10^{12} sec^{-1}, which would correspond to a Debye temperature of 300°K assuming that this may be the maximum frequency in the structure. This value agrees well with the range of Debye temperature determined by other means, as discussed in Ref. 23.

Another feature to be noted is the parallel trend of the LO and LA branches over a wide range of $q/q_{\max}$ as the zone boundary is approached. A similar trend is noted for the TO$/\!/$ and TA$/\!/$ pair of branches. Seen in its limit, the collapse of both pairs to two acoustical curves would indicate a fixed length of the projection of the basic vector on the basal planes. The trend of the data thus indicates a certain amount of rigidity of the basic vector with respect to stresses parallel to the basal plane. This rigidity appears to be larger in the longitudinal direction, as expected from the geometry of the basic vector and supported by the data from Table III, where $|B_1|<|B_2|$ and $|G_1|<|G_2|$.

[21] R. E. Joynson, Phys. Rev. **94**, 851 (1954).

[22] E. Maliszewski, J. Sosnowski, K. Blinowski, J. Kozubosvski, I. Padlo, and D. Sledziewska, in *Proceedings of the Chalk River Symposium on Inelastic Scattering of Neutrons in Solids and Liquids* (International Atomic Energy Agency, Vienna, 1963), Vol. II, p. 87.

[23] G. A. Alers and J. T. Neighbours, J. Phys. Chem. Solids **7**, 58 (1958).

Motions within the basal planes involve a strain of the basic vector even if its projection on the **c** axis remains constant. To describe such a strain it is necessary to introduce force constants acting between neighboring basal planes. As was found, the Begbie and Born formulation does not adequately describe this situation with the linear combinations of λ and μ, but the additional constants G_1 and G_2 must be introduced. Their presence implies that the coupling between basal planes cannot be thought of as being localized along the basic vector but is extended to a larger crystal volume.

Motion of the basal plane as a whole unit is represented by the branches [0001] T and [0001] L. The only force constants involved here describe coupling between the basal planes only. It is interesting to note that the transverse and longitudinal modes of vibration involve very different frequencies. At $q=0$ the motions of contiguous basal planes are of opposite phase and the difference between the longitudinal and transverse frequencies is greater than a factor of two. Correspondingly, the root-mean-square amplitudes of the normal coordinates associated with these normal modes of vibrations, computed from

$$\langle x^2\rangle=\frac{1}{4\pi^2\nu^2 m}\left(\frac{h\nu}{2}+\frac{h\nu}{\exp h\nu/K_BT-1}\right), \qquad (5)$$

where m is the atomic mass of zinc, are

$$\langle x^2\rangle_T^{1/2}=0.136\ \text{Å};\quad \langle x^2\rangle_L^{1/2}=0.069\ \text{Å}. \qquad (6)$$

This indicates that the tendency towards slippage between planes is greater than the tendency to separate the planes. The easy cleavage of zinc along the basal planes is probably assisted by this.

The branches $[01\bar{1}0]$ TA$\perp$ and $[01\bar{1}0]$ TO$\perp$ are associated with motions which tend to warp the basal planes. These motions tend to change the length of the projection of the basic vector on the **c** axis, while the motions associated with the other four $[01\bar{1}0]$ branches tend to change the projection of the basic vector on the basal plane.

Consideration of the interatomic force constants of Table III indicates:

(1) For the first nearest neighbors, in the basal plane, there is a strong, almost totally central interaction (interatomic-force constant α). Correspondingly, the frequencies of the $[01\bar{1}0]$ L branches are rather high and the structure of the basal plane may be considered to be characterized by a strong individuality within the crystal;

(2) For the second and third nearest neighbors located in a plane at $z=\frac{1}{2}c$ from the basal plane, the interatomic force constants B_1, B_2, G_1, and G_2, which are responsible for the sliding motions parallel to the basal planes, are smaller than the constants B_3 and G_3, which are responsible for the separating motions along the **c** axis. This seems to indicate that separating motions of the basal planes may play a minor role in determining the onset of cleavage in zinc.

The present data has revealed a number of interesting features of the arrangement and extent of interatomic- and interplanar-forces in zinc. The details of the interplanar anisotropy indicates that a study of the exact manner of breakup of the zinc lattice upon melting might be interesting. The anomalous changes in the slope of the $[01\bar{1}0]$ TA$\perp$ branch in the region of $q/q_{\max}=0.65$ and the less pronounced slope variation of the $[01\bar{1}0]$ LO$\perp$ and [0001] L branches in the same region of $q/q_{\max}$ are considered to be outside experimental errors and thus to be real. The data have not yet been taken in sufficiently small increments of $q/q_{\max}$ and at conveniently low energies of the impinging neutrons to discuss the details of these anomalies. Also in view of the theory recently formulated by Harrison,[24,25] further work in this direction is planned for the near future.

Note added in proof. It is interesting to note that the quantity $\sum_j \omega_j^2(\mathbf{q})$[26,27] is constant, within our experimental errors, for the [0001] direction, while it is strongly dependent upon **q** for the $[01\bar{1}0]$ direction. This different behavior supports the strong anisotropy of zinc.

[24] W. A. Harrison, Phys. Rev. **129**, 2503 (1963).
[25] W. A. Harrison, Phys. Rev. **129**, 2512 (1963).
[26] R. Brout, Phys. Rev. **113**, 43 (1959).
[27] H. B. Rosenstock, Phys. Rev. **129**, 1959 (1963).